Chemical Engineering Journal 153 (2009) 175–182

Contents lists available at ScienceDirect

Chemical Engineering Journal

journal homepage: www.elsevier.com/locate/cej

Studies on the oxidation reaction of L-cysteine in a confined matrix of layered double hydroxides

Qiuhua Chen[a], Shuxian Shi[a], Xiaolei Liu[a,b], Lan Jin[a], Min Wei[a,*]

[a] State Key Laboratory of Chemical Resource Engineering, Beijing University of Chemical Technology, Beijing 100029, PR China
[b] Chemical Engineering Department, Zibo Vocational Institute, Zibo 255314, PR China

ARTICLE INFO

Article history:
Received 16 April 2009
Received in revised form 7 June 2009
Accepted 25 June 2009

Keywords:
L-Cysteine
Confined reaction
Layered double hydroxide (LDH)
Kinetic

ABSTRACT

The amino acid L-cysteine (L-Cys) was intercalated into a MgAl layered double hydroxide (LDH), and its oxidation reaction by hexacyanoferrate (III) ($Fe(CN)_6^{3-}$) in the confined region between sheets of LDH has been studied in detail. Based on the measurement results of XRD, Raman and FT-IR, it was found that the interlayer L-Cys was oxidized to cystine by $Fe(CN)_6^{3-}$. Furthermore, the kinetics of this reaction was investigated in batch mode. The influences of initial $Fe(CN)_6^{3-}$ concentration, L-Cys-LDH quantity and reaction temperature on the interlayer oxidation reaction have been studied, respectively. The reaction follows a diffusion-controlled mechanism represented by Crank-Ginstling and Brounshtein kinetic model with the apparent activation energy of 29.93 kJ/mol. Therefore, this layered material may have prospective application as a novel "molecular reactor" for confined chemical reactions.

1. Introduction

Layered double hydroxides (LDHs), also known as hydrotalcite-like compounds or anionic clays, are a class of materials consisting of positively charged brucite-like layers and exchangeable interlayer anions. The general formula for LDHs is $M(II)_{1-x}M(III)_x(OH)_2A_{x/n}{\cdot}mH_2O$, where M^{2+} and M^{3+} are di- and trivalent metal cations occupying octahedral positions within the hydroxide sheets, and A^{n-} is an interlayer anion that compensates for the charge on the layers [1–4]. The attractive feature of such materials is that they serve as a template for the formation of supramolecular structures, which have attracted increasing interest for potential technological applications in the fields of catalysis [5–7], separators [8–10] and synthesis material for organic–inorganic nanocomposites [11,12].

In recent years, considerable attentions have been paid to explore the multifarious functions of LDH materials [13–15]. One of the most interesting features of LDHs is their role as a molecular reactor due to the interlayer confined region. The host layers can impose restrained geometry on the interlayer guests leading to influence control of stereochemistry, rates of reaction and product distributions. Therefore, the study of interlayer chemical reaction and potential applications based on LDH matrix is a rapidly growing field [16,17]. For instance, alkylbenzoates have been synthesized between sheets of LDH by the reaction of benzoate and alkyl halide under dry media conditions. It was reported that the synthesis of anionic benzoate in the galleries of LDH showed higher selectivity and yield, compared with the use of sodium benzoate supported as a salt [18]. In our previous work [19], L-Cys and cystine were intercalated into LDH by the coprecipitation method and the oxidation of intercalated L-Cys by H_2O_2 and Br_2 were also studied, respectively. It was found that H_2O_2 oxidized the interlayer L-Cys to cystine, while the oxidation product of intercalated L-Cys by Br_2 was cysteic acid regardless of the molar ratio of bromine/cysteine, which was rather different from the bulk reaction.

In the present study, we further focus on the kinetics of the oxidation reaction of L-cysteine (L-Cys) by hexacyanoferrate (III) in the confined region of LDH. Although the kinetics of oxidation of L-Cys is fairly well understood in homogeneous system [20], there is a lack of in-depth knowledge on the oxidation reaction of L-Cys in a restricted environment. Because the oxidation of L-Cys is the simplest model for enzymatic reactions in biochemistry, the study on its oxidation reaction in the galleries of LDH could provide a deep understanding of thiols oxidation in the intracellular biological processes. In this work, the oxidation process and reaction products were analyzed by several methods. The influences of initial $Fe(CN)_6^{3-}$ concentration, L-Cys-LDH quantity and reaction temperature on the interlayer reaction have been investigated, respectively. Moreover, four kinetic models based on the shrinking core model were chosen to fit the experimental data, including first- and second-order kinetic model, surface reaction kinetic model, as well as Crank-Ginstling and Brounshtein kinetic model. It was found that the Crank-Ginstling and Brounshtein kinetic model gives the best description for the oxidation process, indicating that the rate

* Corresponding author. Tel.: +86 10 64412131; fax: +86 10 64425385.
E-mail addresses: weimin@mail.buct.edu.cn, weimin-hewei@163.com (M. Wei).

1385-8947/$ – see front matter © 2009 Elsevier B.V. All rights reserved.
doi:10.1016/j.cej.2009.06.034

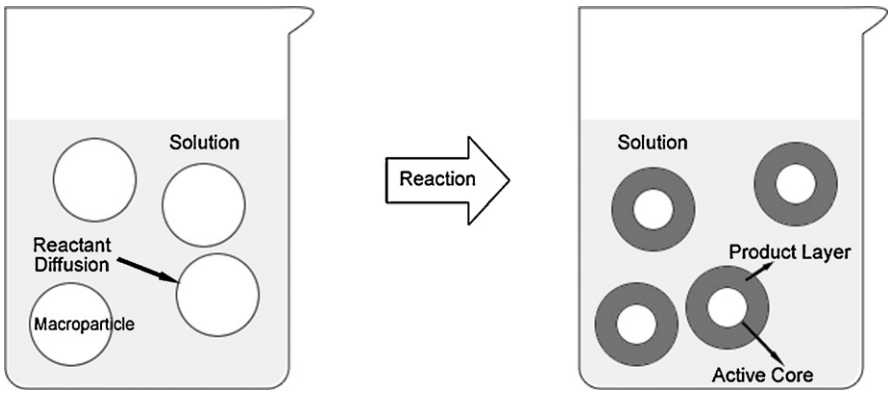

Scheme 1. Schematic representation of the reaction process based on shrinking core model.

of reaction is controlled by the diffusion of $Fe(CN)_6^{3-}$ through the intralamellar of LDH matrix. Therefore, this work gives fundamental understanding on the oxidation reaction of L-Cys in a confined region based on LDH matrix.

2. Experimental

2.1. Preparation of L-Cys-LDH

The L-Cys-LDH was synthesized by the coprecipitation method reported previously [19]. A solution of $Mg(NO_3)_2{\cdot}6H_2O$ (12.8 g, 0.05 mol) and $Al(NO_3)_3{\cdot}9H_2O$ (9.38 g, 0.025 mol) in 100 mL CO_2-free deionized water was slowly added to a solution of L-Cys (4.50 g, 0.0375 mol) and NaOH (8.0 g, 0.2 mol) with vigorous agitation under nitrogen atmosphere. The mixture was aged at 65 °C under a nitrogen atmosphere for 24 h after the solution pH was adjusted to 10.5. The product was washed extensively with deionized water, centrifuged and dried at room temperature under vacuum for a further 24 h.

2.2. Oxidation of L-Cys-LDH by hexacyanoferrate (III)

Oxidation experiments were carried out using a batch method. A 0.01 mol of hexacyanoferrate (III) was dissolved in 100 mL of deionized water and stirred in flask under nitrogen atmosphere. The flask was placed in a water bath to keep the desired reaction temperature throughout the whole experiment. The reaction was initiated by adding the requisite amount of L-Cys-LDH sample. At specified time intervals, 1.0 mL of solution was removed and filtered through a 0.2 μm syringe filter. The concentration of $Fe(CN)_6^{3-}$ was measured momentarily using a UV–vis spectrophotometer at 420 nm. Runs were performed in triplicate. The influences of initial L-Cys-LDH quantity, $Fe(CN)_6^{3-}$ concentration, and temperature of reaction have been tested in kinetic runs.

2.3. Analysis of reaction products

Aliquots of the suspension were taken after 20 min from a reaction of hexacyanoferrate (III) (1.0 mmol/L) with L-Cys-LDH samples. The solid product was obtained by immediate filtration and dried in a vacuum oven at room temperature for 24 h. The product in solution was preprocessing by diluted HCl solution and centrifuged prior to Raman and FT-IR analysis.

2.4. Characterization

The powder X-ray diffraction pattern of the samples were obtained using a Shimadzu XRD-6000 diffractometer with Cu-Kα radiation (40 kV and 30 mA) at a scanning rate of 5° min^{-1}. Fourier transform infrared spectra were recorded using a Vector22 (Bruker) spectrophotometer in the range 4000–400 cm^{-1} with 2 cm^{-1} resolution. The standard KBr disk method (1 mg of sample in 100 mg of KBr) was used. UV–vis spectra were recorded on a Shimadzu UV-2501PC spectrometer in the wavelength range 200–700 nm, and quantitative analysis was performed at 420 nm. Fourier-Transform Raman spectra were recorded in backscattering geometry, using a Renishaw RM2000 NIR-FT Raman spectrometer (excitation wavelength 633 nm, He-Ne laser). The laser power was set at 4.7 mW (at the sample) and typically 32 scans were accumulated. The spectral resolution was 4 cm^{-1}. Analysis of metal element and sulfur was performed by ICP emission spectroscopy on a Shimadzu ICPS-7500 instrument. Carbon, hydrogen, and nitrogen analyses were carried out using an Elementarvario elemental analysis instrument.

3. Kinetic modeling

Because of the strong electrostatic attraction between the LDH layers and interlayer anions, we refer to the fact that a single LDH macroparticle is an agglomerate of spherical crystallites, and the LDH crystallites consist of LDH layers and anions between the sheets [21]. For the sake of simplifying calculation, the LDH crystallites are considered as microspheres, which continuously dispersed in a symmetrical macroparticle.

In order to determine the kinetic parameters and rate controlling step about the heterogeneous reaction between $Fe(CN)_6^{3-}$ and L-Cys-LDH, the experimental data were analyzed on the basis of the shrinking core model [22–24]. According to the conception, the reaction is considered to take place at the active core, and reactant molecules in solution penetrate inside the particle deeply as the oxidation process progresses (as shown in Scheme 1). Corresponding models for the oxidation reaction are summarized in Table 1. In detail, models F1 and F2 are relatively simple models with reaction order of 1 and 2 respectively. They represent the reaction occurring at the surface of macroparticle, hence the rate-determining step is diffusion of fluid film or chemical reaction. Model R3 and R4 describe the case where spherical particles react with a fluid creating a reaction product layer around the unreacted active core. Respectively, model R3 is controlled by the active core surface reaction, as the surface reaction is the rate-determining step. Model

Table 1
Kinetic models list.

Equation	Type	Notation
$kt = -\ln(1-\alpha)$	First-order kinetics	F1
$kt = (1-\alpha)^{-1}$	Second-order kinetics	F2
$kt = 1-(1-\alpha)^{1/3}$	3-D advance of the reaction interface	R3
$kt = 1-2/3\alpha-(1-\alpha)^{2/3}$	Crank-Ginstling and Brounshtein	R4

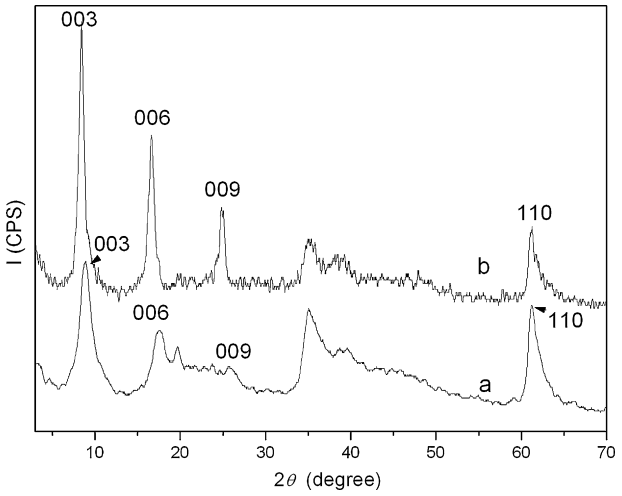

Fig. 1. Powder XRD patterns of (a) L-Cys-LDH, and (b) the reaction product of L-Cys-LDH and $Fe(CN)_6^{3-}$.

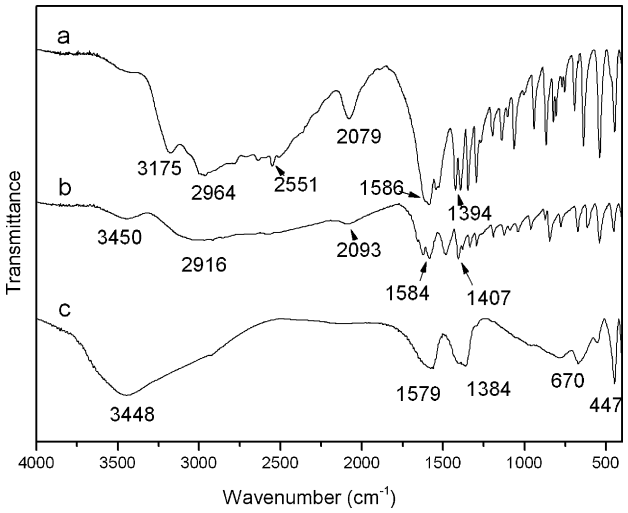

Fig. 2. FT-IR spectra of (a) pristine L-Cys, (b) pristine cystine, and (c) L-Cys-LDH.

R4, an equation originally proposed by Crank-Ginstling and Brounshtein, is retarded by diffusion resistance through the product layer.

The α is conversion of the interlayer L-Cys:

$$\alpha = \frac{C_{0Cys} - C_{Cys}}{C_{0Cys}} \quad (1)$$

where C_{0Cys} and C_{Cys} represent the L-Cys concentration at the beginning and after a certain time of reaction, respectively. The total L-Cys concentration is calculated as

$$C_{Cys} = \frac{m_{Cys}}{M_{Cys} V_L} \quad (2)$$

where m_{Cys} is the mass; M_{Cys} the molar mass and V_L the volume of $Fe(CN)_6^{3-}$ solution. If the reaction follows any of the four kinetic models in Table 1, there must be a linear relationship between the right side of equation and time. Hence the slope of the line is the rate constant. The temperature dependence of the reaction rate constant k can be described by the Arrhenius equation:

$$k = Ae^{-(E_a/RT)} \quad (3)$$

where A is frequency factor; E_a is activation energy of the reaction; R is universal gas constant and T is absolute temperature.

4. Results and discussion

4.1. Characterization of L-Cys-LDH

The powder XRD patterns of L-Cys-LDH and the reaction product of L-Cys-LDH are displayed in Fig. 1, and the basal spacing and lattice parameters are listed in Table 2. In each case, the XRD patterns exhibit the characteristic reflections of the LDH structure with a series of (0 0 l) peaks appearing as narrow, symmetric, strong lines at low angle. The XRD pattern of L-Cys-LDH (Fig. 1a) is similar to that reported previously [19], with an interlayer spacing (d_{003}) of 0.993 nm. The XRD pattern of reaction product of L-Cys-LDH will be discussed in the next section. The chemical composition for L-Cys-LDH is $Mg_{0.67}Al_{0.33}(OH)_{2.00}(C_3H_5NO_2S)_{0.14}(NO_2S)_{0.14}(NO_3)_{0.05}$. It should be noted that the interlayer organic content was calculated from the weight of sulfur by ICP and the co-intercalated nitrate was obtained from the nitrogen content by elemental analysis.

Table 2
Lattice parameters of L-Cys-LDH and the reaction product of L-Cys-LDH and hexacyanoferrate (III).

Lattice parameters (nm)	L-Cys-LDH	Reaction product of L-Cys-LDH and hexacyanoferrate (III)
d_{003}	0.993	1.050
d_{006}	0.503	0.534
d_{009}	0.352	0.357
d_{110}	0.152	0.152
Lattice parameter a	0.304	0.304
Lattice parameter c	3.010	3.200

The FT-IR spectra of the pristine L-Cys, pristine cystine and the intercalated compound L-Cys-LDH are presented in Fig. 2. In the spectra of L-Cys and cystine, the absorption bands at 3175 and 2964 cm^{-1} in Fig. 2a, the strong bands at 3450 and 2916 cm^{-1} along with several bands in the range 2965–2050 cm^{-1} in Fig. 2b are attributed to the ν(C–H) and ν(N–H) stretching vibration absorptions, respectively. The R–COO^- asymmetric and symmetric stretching vibration absorptions are respectively observed at 1586 and 1394 cm^{-1} (Fig. 2a), and 1584 and 1407 cm^{-1} (Fig. 2b). In the case of L-Cys-LDH (Fig. 2c), the spectrum shows a broad absorption band at 3448 cm^{-1} due to the stretching vibration of the hydroxyl group in the LDH layers. In particular, the S–H stretching vibration at 2551 cm^{-1} (Fig. 2a) is absent in the spectrum of L-Cys-LDH (Fig. 2c), indicating that the interlayer L-Cys exists as divalent anion. In addition, the lattice vibration of metal cations Al^{3+} and Mg^{2+} of LDH are noted at 670 cm^{-1} (Fig. 2c).

4.2. Characterization of the reaction products of L-Cys-LDH and hexacyanoferrate (III)

The Raman spectra of $Fe(CN)_6^{3-}$, $Fe(CN)_6^{4-}$, L-Cys-LDH, the solid product and the product extracted from solution are displayed in Fig. 3. Compared with L-Cys-LDH (Fig. 3c), two strong bands centered at 2092 and 2064 cm^{-1} were observed in the spectrum of the solid product (Fig. 3d), which are related to the ν(C≡N) stretching absorptions in $Fe(CN)_6^{4-}$ with A_{1g} and E_g form (shown in Fig. 3b), respectively [25,26]. The band at 552 cm^{-1} (Fig. 3d) is due to the M–O–H bending deformation vibration of LDH layers. In addition, both the characteristic vibrational absorption of the disulfide linkage (S–S) at 493 cm^{-1} and the characteristic absorption of $Fe(CN)_6^{4-}$ at 2134 cm^{-1} (shown in Fig. 3a) were not observed in the solid product, excluding the existence of cystine and $Fe(CN)_6^{3-}$ in LDH matrix. This indicates that only $Fe(CN)_6^{4-}$ formed in the interlayer region of LDH after the oxidation reaction. Fig. 3e displays the product extracted from the solution. An intense absorption band of the disulfide linkage (S–S) at 493 cm^{-1} appears, indicating the formation of oxidation product cystine in the solution. This will be

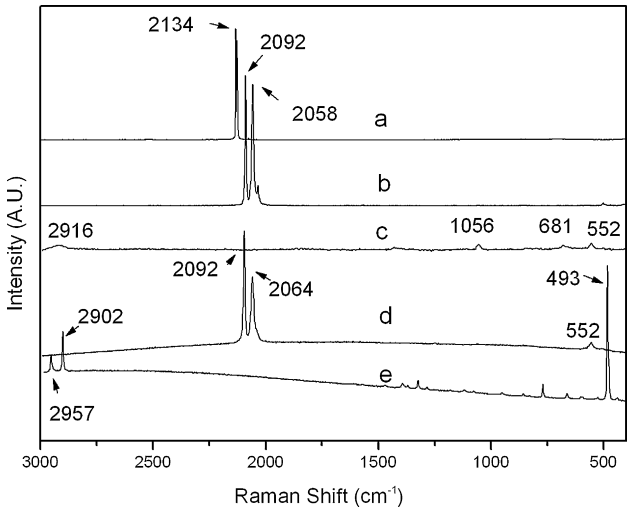

Fig. 3. Raman spectra of (a) $Fe(CN)_6^{3-}$, (b) $Fe(CN)_6^{4-}$, (c) L-Cys-LDH, (d) the solid product, and (e) the product extracted from solution.

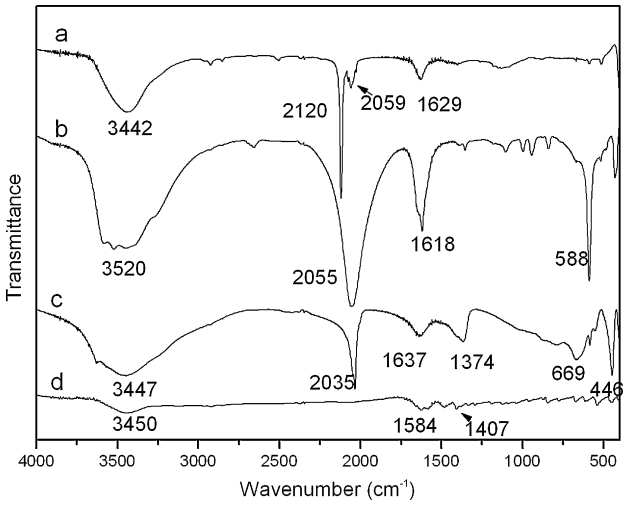

Fig. 4. FT-IR spectra of (a) $Fe(CN)_6^{3-}$, (b) $Fe(CN)_6^{4-}$, (c) the solid product, and (d) the product extracted from solution.

further discussed based on the XRD and FT-IR results in the next section.

The powder XRD pattern for the solid product of the reaction is shown in Fig. 1b. The (0 0 3), (0 0 6), (0 0 9) and (1 1 0) reflections of the oxidation product of L-Cys-LDH by hexacyanoferrate (III) are observed at 8.39°, 16.58°, 24.91° and 61.34°, respectively. Well-ordered (0 0 *l*) series indicates that the hydrotalcite-like structure of the host was maintained. After the oxidation reaction of L-Cys-LDH, the interlayer distance increased to 1.050 nm. This value is different from that of cystine intercalated LDH (1.390 nm) in our previous work [19]. Comparison study between the product and the reported work by Boclair et al. [27] indicates that the pattern of reflections is indicative of a well-ordered, single-phase LDH, namely, LDH ferricyanide. The IR spectra for $Fe(CN)_6^{3-}$, $Fe(CN)_6^{4-}$, the solid product, as well as the product extracted from solution are shown in Fig. 4. The spectrum of the solid product (Fig. 4c) shows a strong band at 2035 cm^{-1}, corresponding to the ν(C≡N) vibration of $Fe(CN)_6^{4-}$ with T_{1u} form [27]. Compared with the pristine $Fe(CN)_6^{4-}$ (2055 cm^{-1}, Fig. 4b), a red-shift of 20 cm^{-1} occurs, as a result of the host–guest interactions between LDH and $Fe(CN)_6^{4-}$. Additionally, a high-frequency ν(O–H) (3447 cm^{-1}, not $Mg(OH)_2$), and a characteristic lattice vibration of LDH at 446 cm^{-1} were also observed (Fig. 4c). Fig. 4d displays the product in solution extracted from filtrate, which is very close to that of pristine cystine (Fig. 2b). The strong band at 3450 cm^{-1} can be attributed to superimposition of ν(N–H) and ν(O–H) vibrations, and the asymmetric and symmetric stretching vibrations of R–COO^- were observed at 1584 and 1407 cm^{-1}. This is in accordance with the results of Raman and XRD. Based on the results above, it can be concluded that the oxidation product of L-Cys-LDH is cystine which dissolves in solution, while the reduction product is $Fe(CN)_6^{4-}$ which is accommodated in the interlayer region of LDH matrix.

As a result, the reaction between L-Cys-LDH and $Fe(CN)_6^{3-}$ can be described by Eq. (4): two molecules of L-Cys transforms to one cystine, and then diffuses from the interlayer region to solution, resulting in the decrease of interlayer negative charge; the reduction product $Fe(CN)_6^{4-}$ with high affinity to LDH sheets exists in the LDH galleries to compensate for the positive charge of the LDH layers.

$$2^-OOCCHNH_2CH_2S^-/LDH + 2Fe(CN)_6^{3-} \rightarrow {}^-OOCCHNH_2CH_2SSCH_2NH_2CHCOO^- + 2Fe(CN)_6^{4-}/LDH \quad (4)$$

Hence, the following steps could be proposed for the heterogeneous reaction between L-Cys-LDH and $Fe(CN)_6^{3-}$: (1) $Fe(CN)_6^{3-}$ molecule transfers from the bulk solution to the boundary sur-

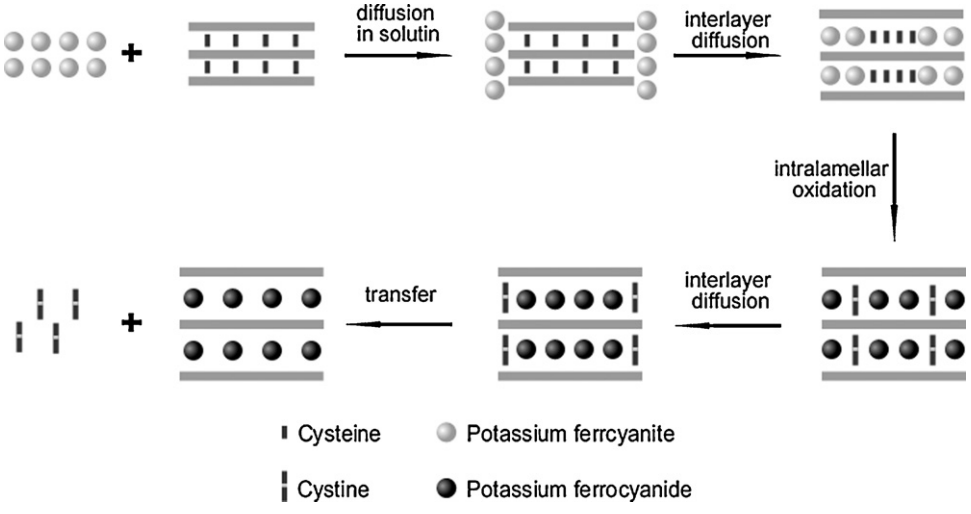

Scheme 2. Schematic representation of the oxidation process of L-Cys in LDH matrix by hexacyanoferrate (III).

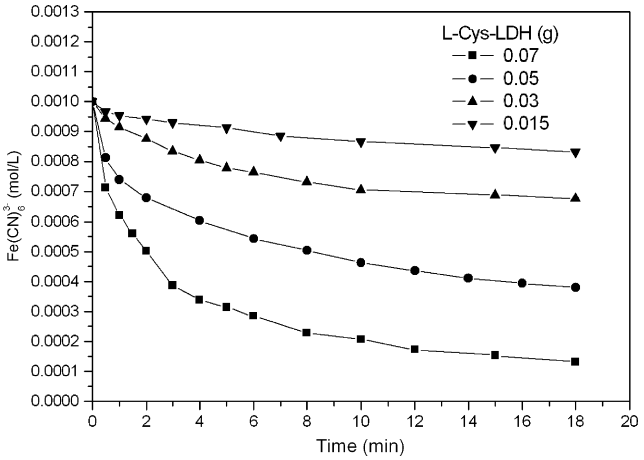

Fig. 5. Effect of initial L-Cys-LDH quantity on the kinetics for the oxidation reaction (V_L = 100 mL, T = 30 °C, $C_{Fe(CN)6^{3-}}$ = 1.0 mmol/L).

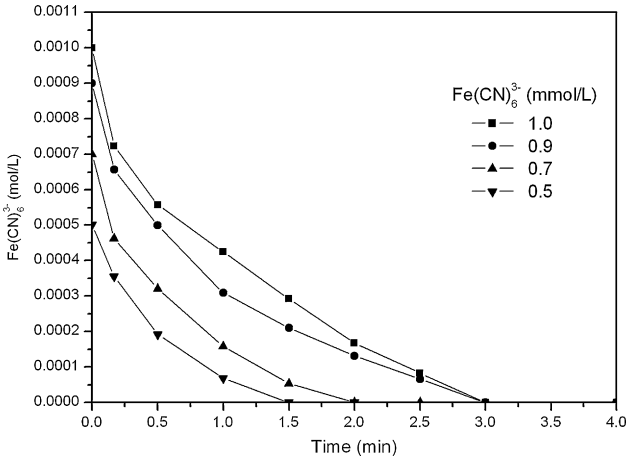

Fig. 7. Effect of initial $Fe(CN)_6^{3-}$ concentration on the interlayer oxidation reaction (V_L = 100 mL, T = 30 °C, $w_{L\text{-}Cys\text{-}LDH}$ = 0.1 g).

face of the L-Cys-LDH particle; (2) $Fe(CN)_6^{3-}$ diffuses into the interlayer region of LDH; (3) $Fe(CN)_6^{3-}$ oxidizes L-Cys to cystine, and at the same time, $Fe(CN)_6^{3-}$ is reduced to $Fe(CN)_6^{4-}$; (4) the oxidation product cystine diffuses to the edges of LDH particle; (5) cystine enters into solution from the boundary surface of LDH, leaving $Fe(CN)_6^{4-}$ in the LDH galleries (as shown in Scheme 2).

4.3. Study on the reaction kinetics

4.3.1. Effect of initial L-Cys-LDH quantity

Fig. 5 displays the reaction rate curves using different L-Cys-LDH quantity (0.015–0.07 g). It was found that the reaction rate increases with increasing L-Cys-LDH quantity, mainly due to the increase in the total surface of LDH particles. Fig. 6 displays the fitting results of experimental data obtained with different L-Cys-LDH quantity, by using the four kinetic models respectively. The corresponding kinetic parameters are summarized in Table 3. It can be seen from Table 3 that the regress coefficients (R^2) for R4 kinetic model are larger than those of other three models. The results show that the R4 model can be used to describe the reaction process satisfactorily, indicating that the reaction is controlled by diffusion of $Fe(CN)_6^{3-}$ through the interlayer region of LDH matrix.

4.3.2. Effect of initial $Fe(CN)_6^{3-}$ concentration

To study the influence of initial concentration of $Fe(CN)_6^{3-}$ on the reaction kinetics, its concentrations within the range 0.5–1.0 mmol/L were investigated. Note that at low initial $Fe(CN)_6^{3-}$ concentration, ferricyanide ions were almost consumed completely (Fig. 7). Therefore, the overall reaction process was not influenced by external mass transfer diffusion [28]. It can be seen from Fig. 8 that Model R4 does not fit well with the experimental data for the whole range of reaction, while Model R3 shows a good agreement with experiment. At low $Fe(CN)_6^{3-}$ concentration, $Fe(CN)_6^{3-}$

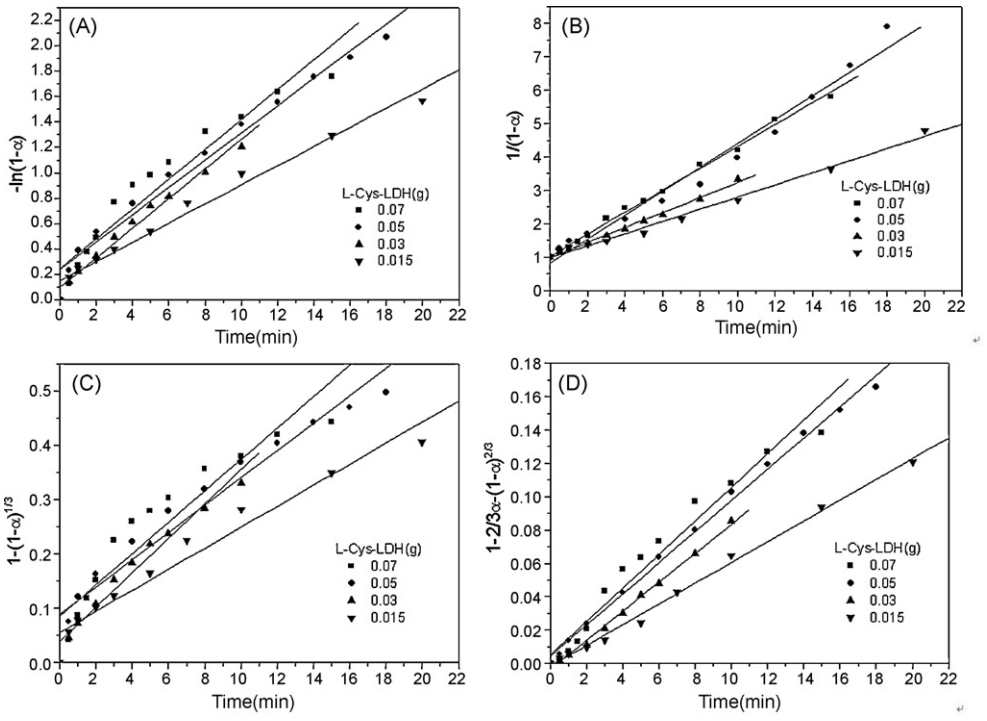

Fig. 6. Effect of initial L-Cys-LDH quantity on the kinetics for the oxidation reaction. Experimental data fitted to (A) F1 model, (B) F2 model, (C) R3 model and (D) R4 model.

Table 3
Experimental conditions, kinetic parameters and regress coefficient of the four kinetic models.

Run no.	$C_{Fe(CN)6}^{3-}$ (mol/L)	$w_{L\text{-}Cys\text{-}LDH}$ (g)	T (K^{-1})	F1		F2	
				k_1 (min^{-1})	R^2	k_2 [(mol/L) $^{-1}$ (min^{-1}]	R^2
1	0.001	0.07	303	0.1172	0.9633	0.3277	0.9979
2	0.001	0.05	303	0.1071	0.9894	0.3572	0.9882
3	0.001	0.03	303	0.1163	0.9916	0.2244	0.9973
4	0.001	0.015	303	0.0754	0.9898	0.1822	0.9957
5	0.001	0.1	303	0.0151	0.9885	0.0623	0.8981
6	0.0009	0.1	303	0.0163	0.9961	0.0723	0.9165
7	0.0007	0.1	303	0.0271	0.9931	0.1233	0.9174
8	0.0005	0.1	303	0.0329	0.9976	0.0219	0.9737
9	0.001	0.05	293	0.0705	0.9851	0.1463	0.9911
10	0.001	0.05	303	0.1071	0.9894	0.3572	0.9882
11	0.001	0.05	313	0.1151	0.9885	0.8241	0.8979

Run no.	$C_{Fe(CN)6}^{3-}$ (mol/L)	$w_{L\text{-}Cys\text{-}LDH}$ (g)	T (K^{-1})	R3		R4	
				k_3 [(mol/L)$^{1/3}$ (min^{-1}]	R^2	k_4 [(mol/L)$^{2/3}$ (min^{-1}]	R^2
1	0.001	0.07	303	0.02887	0.9397	0.01004	0.9823
2	0.001	0.05	303	0.02517	0.9241	0.00935	0.9982
3	0.001	0.03	303	0.03177	0.9827	0.00869	0.9978
4	0.001	0.015	303	0.01933	0.9779	0.00622	0.9977
5	0.001	0.1	303	0.00344	0.9918	0.00128	0.9848
6	0.0009	0.1	303	0.00363	0.9913	0.00137	0.9968
7	0.0007	0.1	303	0.00603	0.9935	0.00224	0.9899
8	0.0005	0.1	303	0.00791	0.9991	0.00549	0.9814
9	0.001	0.05	293	0.01883	0.9741	0.00551	0.9978
10	0.001	0.05	303	0.02517	0.9724	0.00935	0.9982
11	0.001	0.05	313	0.02919	0.9715	0.01205	0.9973

was consumed completely by reacting with L-Cys adsorbed on the surface of LDH particles. Therefore the surface reaction is the rate-determining step under this condition.

4.3.3. Effect of temperature

The effect of temperature on the rate of interlayer oxidation reaction was examined in the range 20–40 °C, under the conditions of 0.05 g L-Cys-LDH and 1.0 mmol/L $Fe(CN)_6^{3-}$. As seen from Fig. 9, the concentration of $Fe(CN)_6^{3-}$ decreases with the increase of reaction time, and the reaction rate increases upon increasing temperature. The conversion of L-Cys (α) after 10 min reached 40%, 50% and 55% for 20, 30 and 40 °C, respectively, indicating that the reaction can be accelerated by raising the temperature. Fig. 10 shows the fitting results of the experimental data obtained at different temperatures

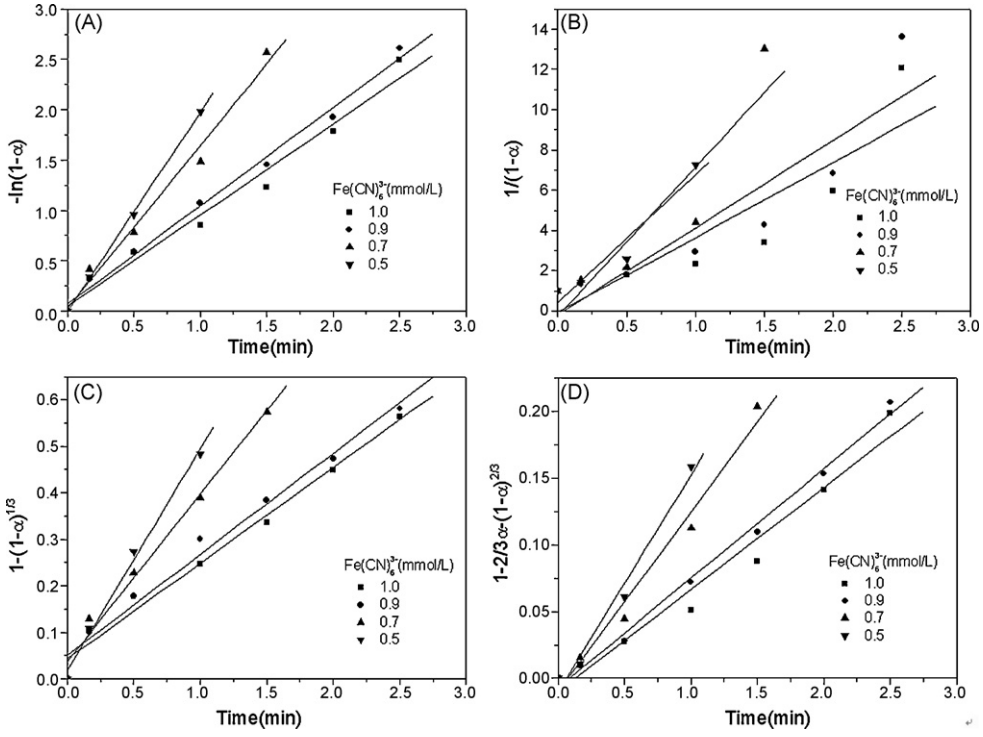

Fig. 8. Effect of initial $Fe(CN)_6^{3-}$ concentration on the kinetics for the oxidation reaction. Experimental data fitted to (A) F1 model, (B) F2 model, (C) R3 model and (D) R4 model.

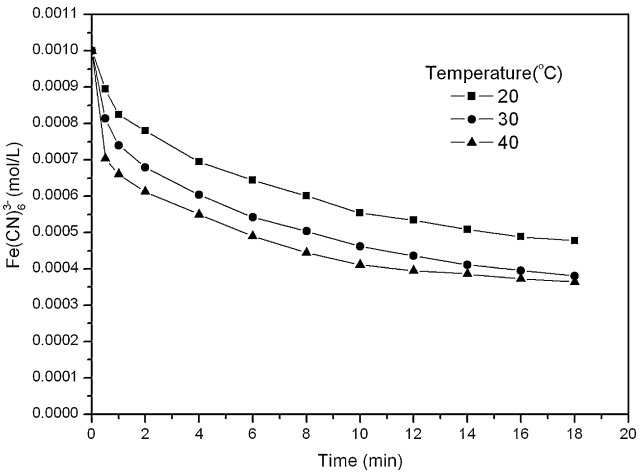

Fig. 9. Effect of temperature on the kinetics of the oxidation reaction (V_L = 100 mL, $w_{L\text{-}Cys\text{-}LDH}$ = 0.05 g, $C_{Fe(CN)6^{3-}}$ = 1.0 mmol/L).

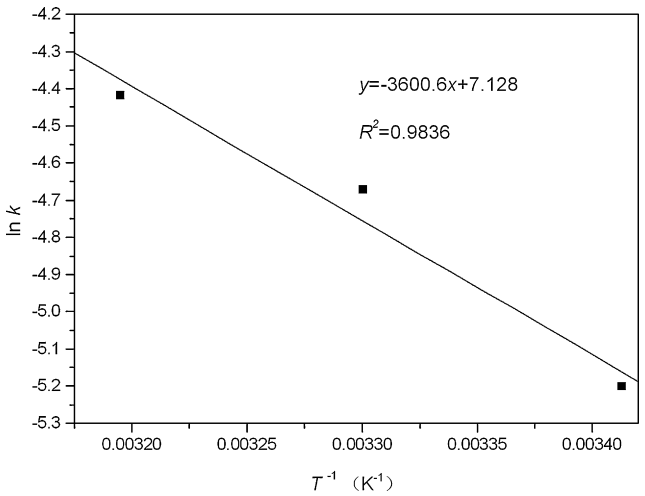

Fig. 11. Arrhenius plot for the oxidation reaction of L-Cys-LDH by $Fe(CN)_6^{3-}$.

based on the four kinetic models respectively. It can be seen from Table 3 that the R4 kinetic model is in good agreement with experiment. The apparent rate constants (k) were calculated from slope of the straight lines for the four models. Using the apparent rate constants obtained by application of R4, the Arrhenius plot ($\ln k$ vs. $1/T$) was obtained (Fig. 11) and the activation energy was calculated to be 29.93 kJ/mol. According to the reports of Ho et al. [29], Lazaridis and Asouhidou [30,31], the diffusion-controlled process has a typical activation energy (E_a) of 25–30 kJ/mol, whereas the E_a of a reaction-controlled process exhibits a value >40 kJ/mol. The value of E_a in this work also confirms that this reaction is controlled by diffusion of $Fe(CN)_6^{3-}$ through the interlayer region of LDH matrix.

5. Conclusions

In this work, L-Cys has been intercalated into LDH galleries in order to study its oxidation reaction with hexacyanoferrate (III) in a confined region. FT-Raman, FT-IR and XRD measurements provide a detailed understanding of the oxidation process for L-Cys between sheets of LDH. It was proposed that the oxidation progress involves five steps: (1) the diffusion of $Fe(CN)_6^{3-}$ in the solution; (2) the diffusion of $Fe(CN)_6^{3-}$ into the LDH galleries; (3) the intralamellar oxidation reaction; (4) the interlayer diffusion of the oxidation product cystine; (5) the transfer of cystine from LDH into solution. Furthermore, the kinetics of this reaction was investigated in detail. The reaction kinetics can be successfully described by Crank-Ginstling and Brounshtein kinetic model with the E_a value of

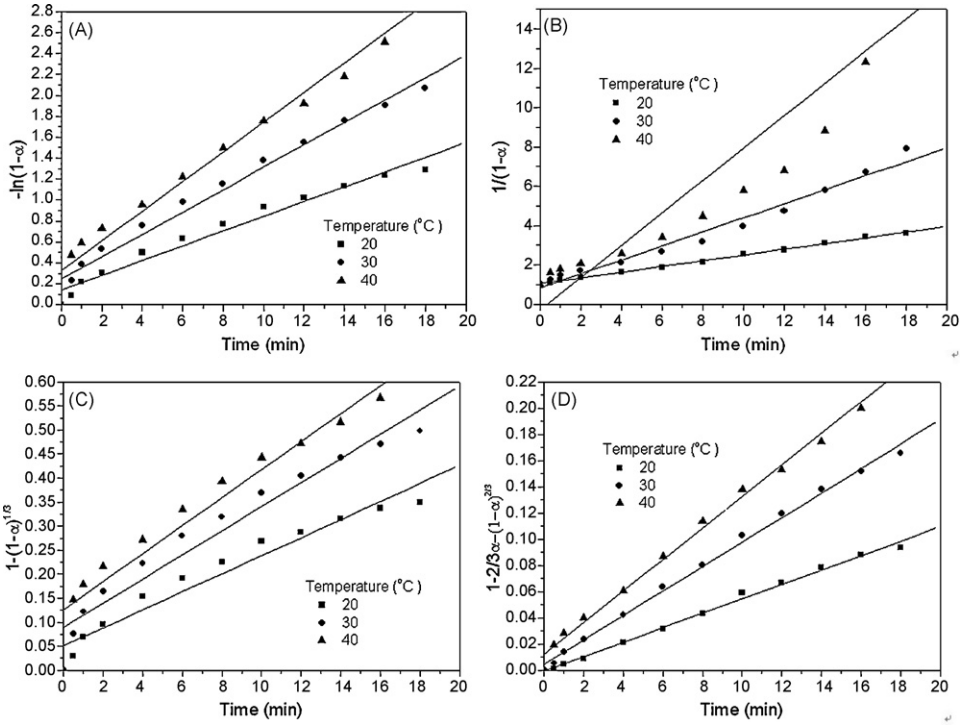

Fig. 10. Effect of temperature on the kinetics for the oxidation reaction. Experimental data fitted to (A) F1 model, (B) F2 model, (C) R3 model and (D) R4 model.

29.93 kJ/mol, indicating an interlayer diffusion-controlled reaction. Therefore, this work not only gives fundamental understanding on the reaction features of L-Cys in a confined region based on LDH matrix, but also provides new opportunities for molecular reactions on the nanoscale of inorganic LDH hybrids and for their use in synthesis and separation applications.

Acknowledgements

This project was supported by the National Natural Science Foundation of China, the 111 Project (Grant No.: B07004), the 973 Program (Grant No.: 2009CB939802) and the Program for Changjiang Scholars and Innovative Research Team in University (Grant No.: IRT0406).

References

[1] D.G. Evans, R.C.T. Slade, Structural aspects of layered double hydroxides, Structure and Bonding (Berlin) 119 (2006) 1–87.
[2] F. Leroux, C. Taviot-Guého, Fine tuning between organic and inorganic host structure: new trends in layered double hydroxide hybrid assemblies, Journal of Materials Chemistry 15 (2005) 3628–3642.
[3] G.R. Williams, D. O'Hare, Towards understanding, control and application of layered double hydroxide chemistry, Journal of Materials Chemistry 16 (2006) 3065–3074.
[4] I.K. Aamir, D. O'Hare, Intercalation chemistry of layered double hydroxides: recent developments and applications, Journal of Materials Chemistry 12 (2002) 3191–3198.
[5] B.F. Sels, D.E. De Vos, P.J. Grobet, F. Pierard, F.K. Mesmaeker, P.A. Jacobs, Molybdate- and tungstate-exchanged layered double hydroxides as catalysts for $^1O_2$ formation: characterization of reactive oxygen species and a critical evaluation of $^1O_2$ detection methods, Journal of Physical Chemistry B 103 (1999) 11114–11123.
[6] B.F. Sels, D.E. De Vos, P.A. Jacobs, Kinetics of the oxygenation of unsaturated organics with singlet oxygen generated from H_2O_2 by a heterogeneous molybdenum catalyst, Journal of the American Chemical Society 129 (2007) 6916–6926.
[7] M. Verïonica, B. Graciela, A. Norma, L. Miguel, Ethanol steam reforming using Ni(II)-Al(III) layered double hydroxide as catalyst precursor: kinetic study, Chemical Engineering Journal 138 (2008) 602–607.
[8] J.M. Morris, S. Jin, K. Cui, Removal of endocrine active compounds using layered double hydroxide material, Chemical Engineering Journal 145 (2008) 160–163.
[9] M.K. Ram Reddy, Z.P. Xu, G.Q. Lu, J.C. Diniz da Costa, Effect of SO_x adsorption on layered double hydroxides for CO_2 capture, Industrial and Engineering Chemistry Research 47 (2008) 7357–7360.
[10] A.M. Fogg, V.M. Green, H.G. Harvey, D. O'Hare, New separation science using shape-selective ion exchange intercalation chemistry, Advanced Materials 11 (1999) 1466–1469.
[11] F. Leroux, J.P. Besse, Polymer interleaved layered double hydroxide: a new emerging class of nanocomposites, Chemistry of Materials 13 (2001) 3507–3515.
[12] L. Desigaux, M.B. Belkacem, P. Richard, J. Cellier, P. Léone, L. Cario, F. Leroux, C. Taviot-Guého, B. Pitard, Self-assembly and characterization of layered double hydroxide/DNA hybrids, Nano Letters 6 (2006) 199–204.
[13] A.I. Khan, L.X. Lei, A.J. Norquist, D. O'Hare, Intercalation and controlled release of pharmaceutically active compounds from a layered double hydroxide, Chemical Communications (2001) 2342–2343.
[14] N. Iyi, Y. Ebina, T. Sasaki, Water-swellable MgAl-LDH (layered double hydroxide) hybrids: synthesis, characterization, and film preparation, Langmuir 24 (2008) 5591–5598.
[15] J.J. Yu, Y.X. Tao, C.C. Liu, Z.P. Hao, Z.P. Xu, Novel NO trapping catalysts derived from Co-Mg/X-Al (X = Fe, Mn, Zr, La) hydrotalcite-like compounds, Environmental Science and Technology 41 (2007) 1399–1404.
[16] A. Illaik, C. Taviot-Guého, J. Lavis, S. Commereuc, V. Verney, F. Leroux, Unusual polystyrene nanocomposite structure using emulsifier-modified layered double hydroxide as nanofiller, Chemistry of Materials 20 (2008) 4854–4860.
[17] G. Carja b, Y. Kameshima, K. Okada, Nanoparticles of iron and vanadium oxides supported on iron substituted LDHs: synthesis, textural characterization and their catalytic behavior in ethylbenzene dehydrogenation, Microporous and Mesoporous Materials 115 (2008) 541–547.
[18] V. PreÂvot, B. Casal, E. Ruiz-Hitzky, Intracrystalline alkylation of benzoate ions into layered double hydroxides, Journal of Materials Chemistry 11 (2001) 554–560.
[19] M. Wei, Z.Y. Shi, D.G. Evans, X. Duan, Study on the intercalation and interlayer oxidation transformation of L-Cys in a confined region of layered double hydroxides, Journal of Materials Chemistry 16 (2006) 2102–2109.
[20] J. Darkwa, R. Olojo, E. Chikwana, R.H. Simoyi, Antioxidant chemistry: oxidation of L-Cys and its metabolites by chlorite and chlorine dioxide, Journal of Physical and Chemical A 108 (2004) 5576–5587.
[21] X.L. Liu, M. Wei, F. Li, X. Duan, Intraparticle diffusion of 1-phenyl-1,2-ethanediol in layered double hydroxides, AIChE Journal 6 (2007) 1591–1600.
[22] C.F. Dickinson, G.R. Heal, Solid-liquid diffusion controlled rate equations, Thermochimica Acta 340 (1999) 89–103.
[23] H. Markus, S. Fugleberg, D. Valtakari, T. Salmi, D.Y. Murzin, M. Lahtinen, Kinetic modelling of a solid-liquid reaction: reduction of ferric iron to ferrous iron with zinc sulphide, Chemical Engineering Science 59 (2004) 919–930.
[24] J.J.M. Órfão, F.G. Martins, Kinetic analysis of thermogravimetric data obtained under linear temperature programming: a method based on calculations of the temperature integral by interpolation, Thermochimica Acta 390 (2002) 195–211.
[25] J.T. Kloprogge, M. Weier, I. Crespo, M.A. Ulibarri, C. Barriga, V. Rives, W.N. Martens, R.L. Frost, Intercalation of iron hexacyano complexes in Zn, Al hydrotalcite. Part 2. A mid-infrared and Raman spectroscopic study, Journal of Solid State Chemistry 177 (2004) 1382–1387.
[26] R.L. Frost, A.W. Musumeci, J. Bouzaid, M.O. Adebajo, W.N. Martens, The kloprogge intercalation of hydrotalcites with hexacyanoferrate (II) and (III)—a thermoRaman spectroscopic study, Journal of Solid State Chemistry 178 (2005) 1940–1948.
[27] J.W. Boclair, P.S. Braterman, B.D. Brister, Z. Wang, F. Yarberry, Physical and chemical interactions between MgAl layered double hydroxide and hexacyanoferrate, Journal of Solid State Chemistry 161 (2001) 249–258.
[28] L. Lv, J. He, M. Wei, D.G. Evans, Z.L. Zhou, Treatment of high fluoride concentration water by MgAl-CO_3 layered double hydroxides: kinetic and equilibrium studies, Water Research 41 (2006) 1534–1542.
[29] Y.S. Ho, G. Mckay, Sorption of dye from aqueous solution by peat, Chemical Engineering Journal 70 (1998) 115–124.
[30] N.K. Lazaridis, D. Asouhidou, Kinetics of sorption removal of chromium (VI) from aqueous solutions by calcined MgAl-CO_3 hydrotalcite, Water Research 37 (2003) 2875–2882.
[31] N.K. Lazaridis, T.A. Pandi, K.A. Matis, Chromium (VI) removal from aqueous solutions by MgAl-CO_3 hydrotalcite: sorption-desorption kinetic and equilibrium studies, Industrial and Engineering Chemistry Research 43 (2004) 2209–2215.